Supporting Information

Water-stable perovskite nanotube array with enhanced transport of charge carriers induced by functionalized polyoxometalate for highly-efficient photoreduction of uranium(VI)

Yanli Yang[a#], Keke Guo[a,b#], Xue Bai[a], Maochun Zhu[a], Siyue Wang[a], and Shuxia Liu[a*]

[a]*Key Laboratory of Polyoxometalate and Reticular Material Chemistry of Ministry of Education, Faculty of Chemistry, Northeast Normal University, Changchun, Jilin 130024, P. R. China*

[b]*Key Laboratory of Eco-Functional Polymer Materials of the Ministry of Education, College of Chemistry and Chemical Engineering, Northwest Normal University, Lanzhou, Gansu 730070, P.R. China*

[#]*Y. Yang and K. Guo contributed equally to this work.*

Email: liusx@nenu.edu.cn

[*] Correspondence to S. L., Email: *liusx@nenu.edu.cn*

Experimental

Materials and methods.

All chemical reagents and solvents were available commercially and used without further purification. $PbBr_2$ (99.99%) and hexamethylenetetramine hydrobromide (HMTA) (99%) were purchased from Energy Chemical. $H_3PW_{12}O_{40}$ (99%) and Stearyltrimethylammonium Bromide (STAB, 99%) were purchased from Aladdin.

Metal elemental analyses were collected by a Leaman inductively coupled plasma (ICP) spectrometer. Powder X-ray diffraction (PXRD) patterns were recorded using Cu Kα radiation (λ = 1.54056 Å) in the range 2θ = 5-50° at 293 K on a Philips X'Pert-MPD instrument. IR spectrum was recorded on an Alpha Centaurt FT/IR spectrometer using a KBr pellet in the frequency range of 2000-600 cm^{-1}. X-ray photoelectron spectroscopy (XPS) spectra was recorded on a Thermo X-ray photoelectron spectrometer. Raman spectra were performed by a high-resolution laser Raman spectrometer (Horiba LabRAM HR Evolution). The morphologies and EDS mapping of the samples were performed on a field emission scanning electron microscope (Hitachi SU-8000 FE-SEM). The solid diffuse reflectance UV-vis spectra of compound 1 was measured on a Cary7000 UV-Vis-NIR Spectrophotometer from 200 to 800 nm at room temperature. A barium sulfate ($BaSO_4$) pellet was used as the standard with 100% reflectance. The steady-state photoluminescence (PL) emission spectroscopy and time-resolved photoluminescence (TRPL) spectra were measured by FLS980 with a 375 nm and 470 nm excitation light, respectively. The photoelectrochemical experiments were performed using a CHI 660 electrochemical workstation (Shanghai Chenhua

Instrument Corp. China) at room temperature. A three-electrode system was employed in a quartz cell with a Pt wire as the counter electrode, a saturated calomel electrode (SCE) as the reference electrode, and the composite film-assembled FTO glass as the working electrode. The illumination area of working electrodes was set constant at 1.0 × 1.0 cm^2. The transient photocurrent experiment was carried out at a constant bias of 0.5 V under simulated sunlight irradiation conditions (300 W Xenon arc lamp, AM 1.5G, 100mW·cm^{-2}) upon on-off cycling irradiation. Mott-Schottky plots was collected by measuring Impedance-Potential curves at the fixed frequency of 1000 Hz. The obtained potential (vs. SCE) was converted to E_{RHE} (E_{NHE} at pH = 0) by the equation $E_{RHE} = E_{SCE} + 0.0592pH + 0.241$. The space charge-limited currents (SCLC) measurements were obtained by measuring the I-V curves using a Keithley 2400 source measure unit instrument (Tektronix) using electron-only device.

Fabrication of $(HMTA)_3Pb_2Br_7$@STA-PW_{12} and $(HMTA)_3Pb_2Br_7$ electron-only devices.

First, 200 mg of $(HMTA)_3Pb_2Br_7$@STA-PW_{12} and $(HMTA)_3Pb_2Br_7$ samples were ground into powder. Then, wafers (diameter: 13 mm) were obtained by processing in a machine for 8 min at 280 MPa. Electron-transporting layers were constructed on the both surface of these two wafers by depositing 8 nm BCP, followed by depositing 20 nm Cu cathode under 5 × 10^{-4} Pa. Finally, the electron-only device with structure of Cu/BCP/wafer/BCP/Cu was fabricated.

Density functional theory (DFT) calculations

The calculations were carried out using the DMOL3 (Density Functional Theory based Quantum Chemistry) software package. The Perdew-Burke-Ernzerhof (PBE)

functional was used within the generalized gradient approximation (GGA). The double numerical plus polarization (DNP) basis set was employed for all atoms in the cluster. The orbital cutoff was set to 3.5 Å to ensure accurate treatment of the electron density near the cluster boundary.

The energy convergence criterion was set to 10 e^{-5} eV/atom, the force convergence criterion was set to 0.002 eV/Å, and the maximum displacement criterion for geometry optimization was set to 0.005 Å. All calculations included spin polarization to accurately describe the magnetic properties of the system. For the geometry optimization, the BFGS algorithm was used.

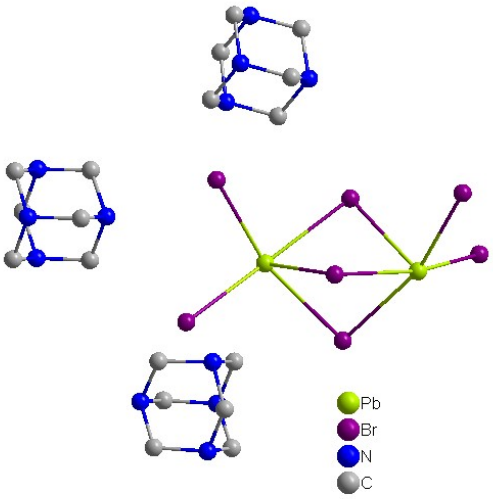

Fig. S1 basic structural motif of $(HMTA)_3Pb_2Br_7$.

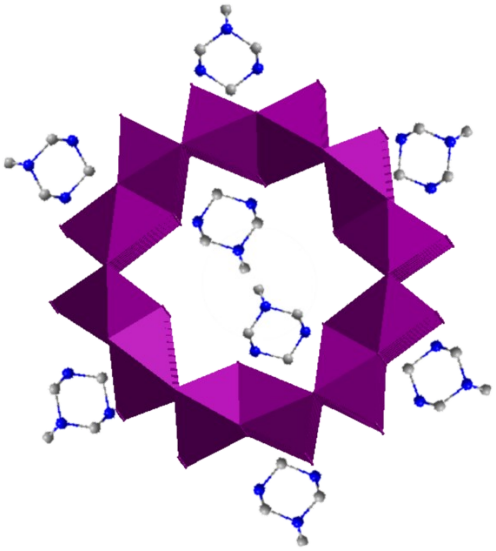

Fig. S2 Rugged rings of $(HMTA)_3Pb_2Br_7$.

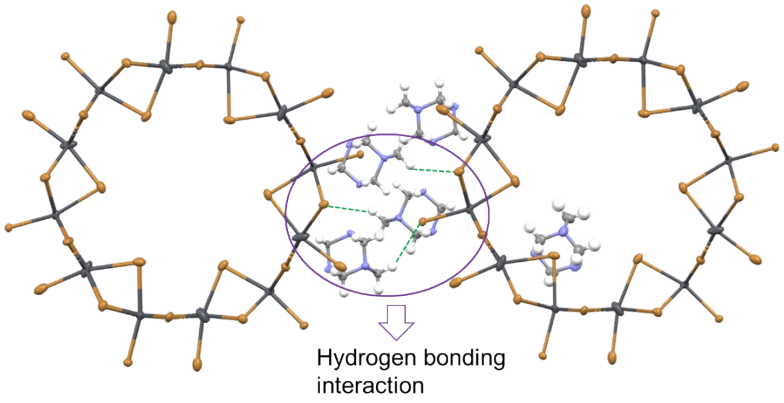

Fig. S3 Hydrogen bonding interactions between adjacent $(HMTA)_3Pb_2Br_7$.

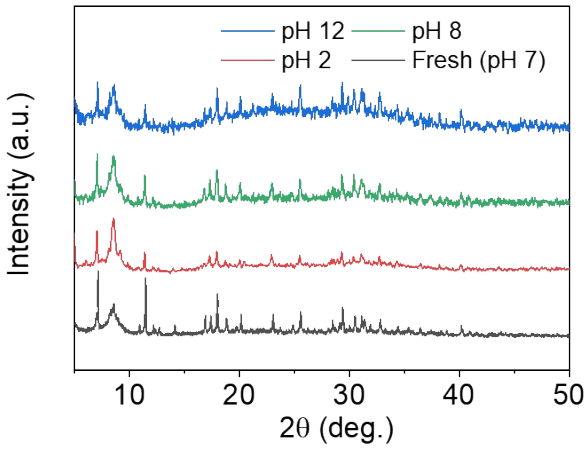

Fig. S4 PXRD patterns of $(HMTA)_3Pb_2Br_7$@STA-PW_{12} at different pH values.

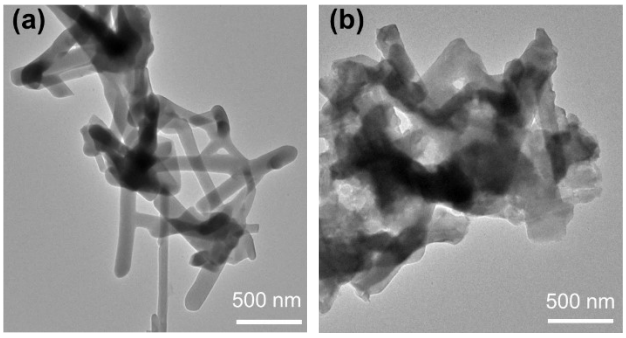

Fig. S5 TEM images of (a) $(HMTA)_3Pb_2Br_7$ and (b) $(HMTA)_3Pb_2Br_7$@STA-PW_{12}.

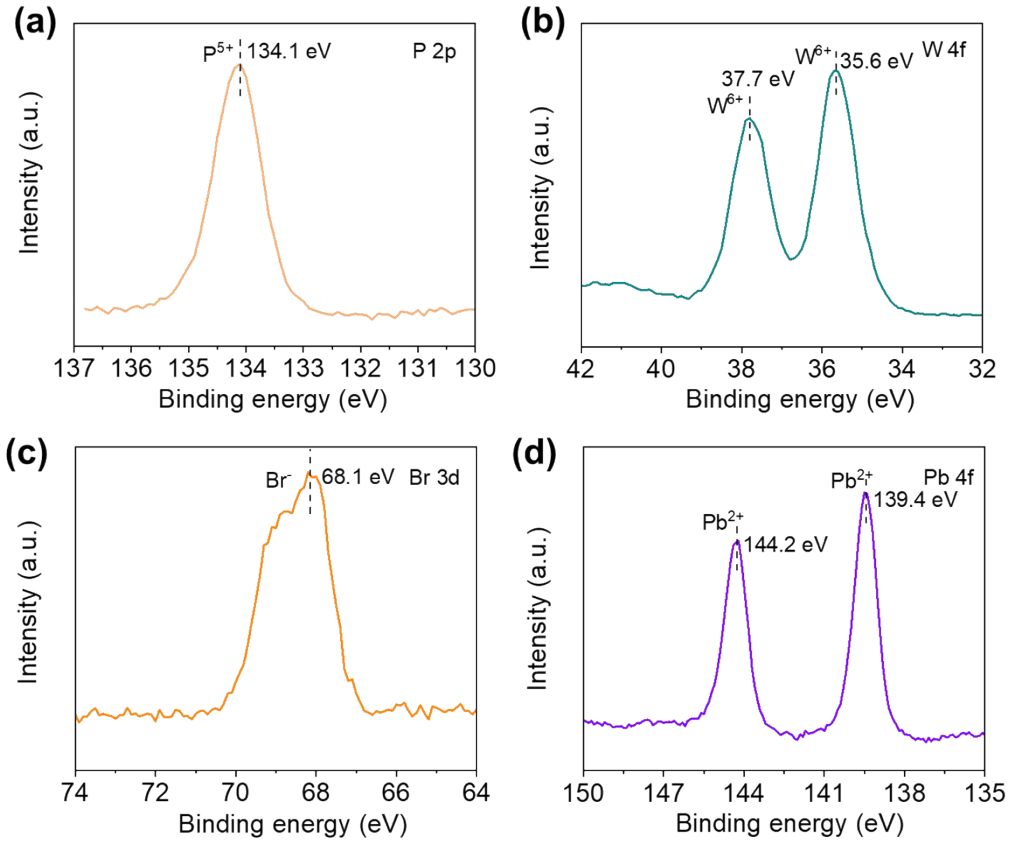

Fig. S6 High-resolution XPS spectra of (a) P 2p, (b) W 4f, (c) Br 3d, (d) Pb 4f of $(HMTA)_3Pb_2Br_7$@STA-PW_{12}.

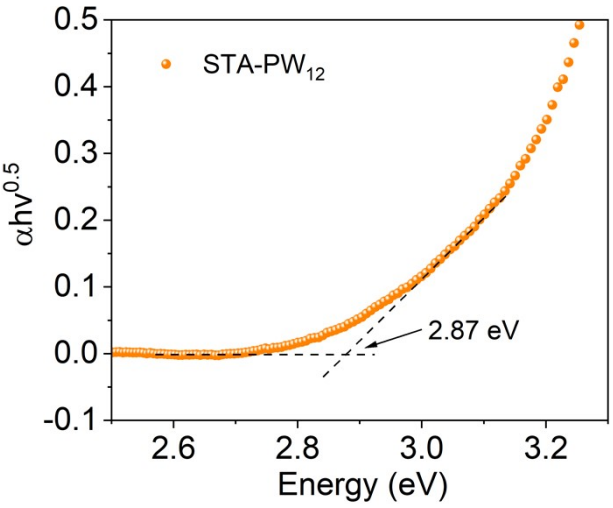

Fig. S7 Tauc plot of STA-PW_{12}.

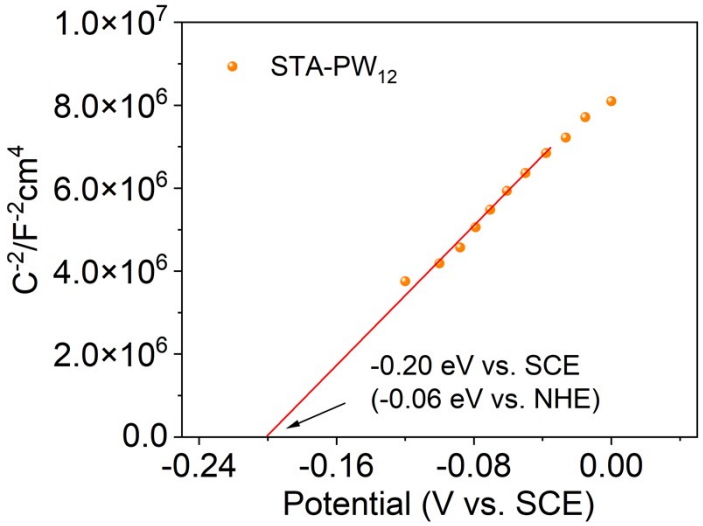

Fig. S8 Mott-Schottky plot of STA-PW_{12}.

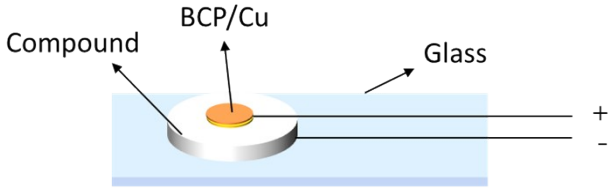

Fig. S9 Cu/BCP/wafer/BCP/Cu device for $(HMTA)_3Pb_2Br_7$ and $(HMTA)_3Pb_2Br_7$@STA-PW_{12} wafers.

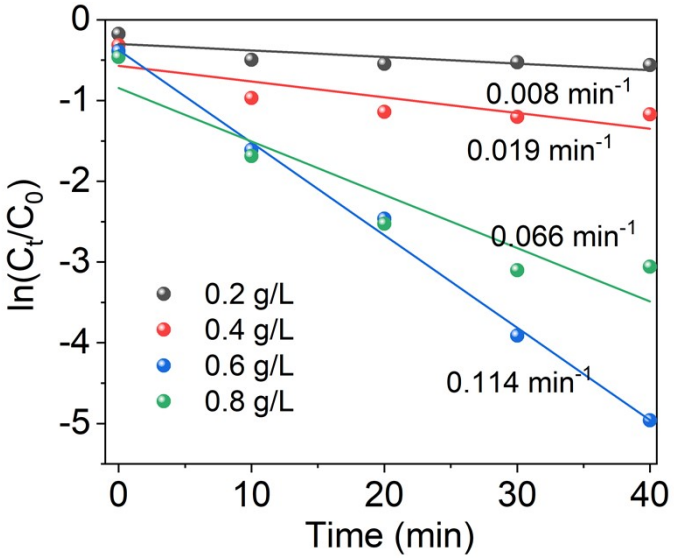

Fig. S10 Curves of $\ln(C_t/C_0)$ vs time at different solid-liquid ratio.

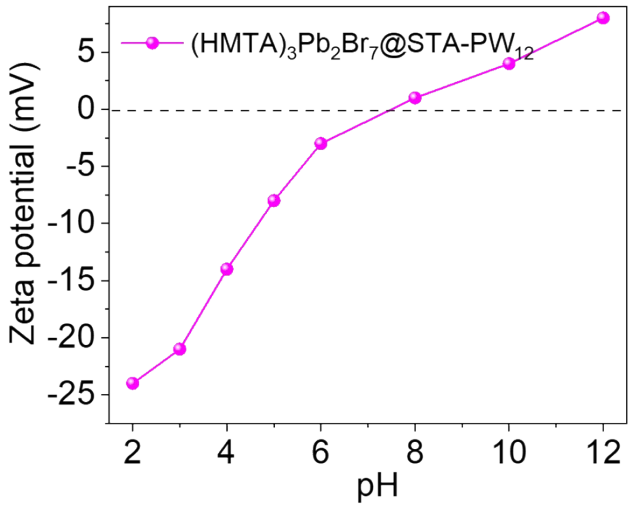

Fig. S11 Zeta potential of $(HMTA)_3Pb_2Br_7$@STA-PW_{12} at different pH values.

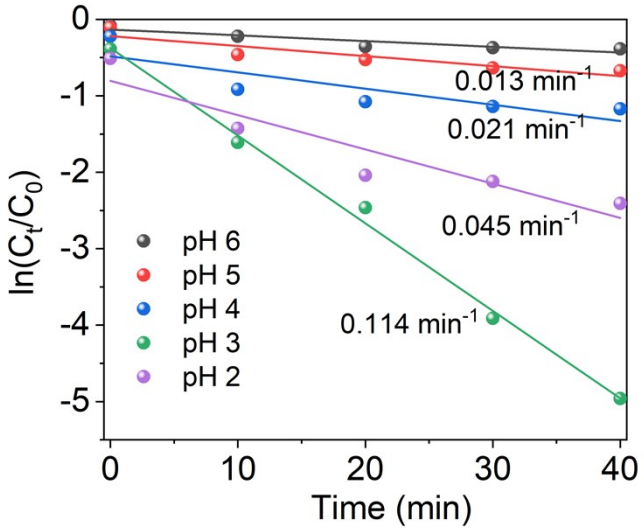

Fig. S12 Curves of $\ln(C_t/C_0)$ vs time at different pH values.

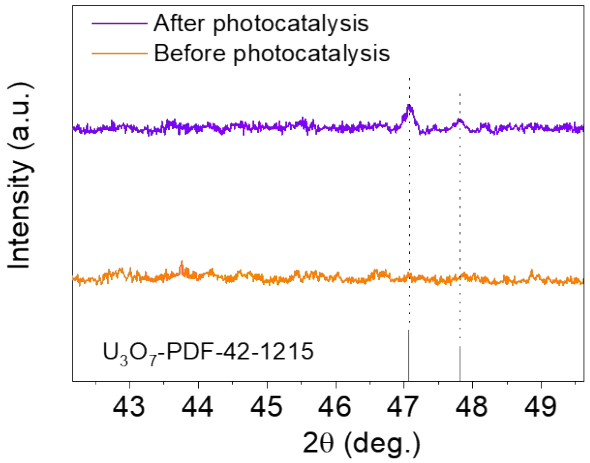

Fig. 13 PXRD patterns of $(HMTA)_3Pb_2Br_7$@STA-PW_{12} before and after photocatalysis.

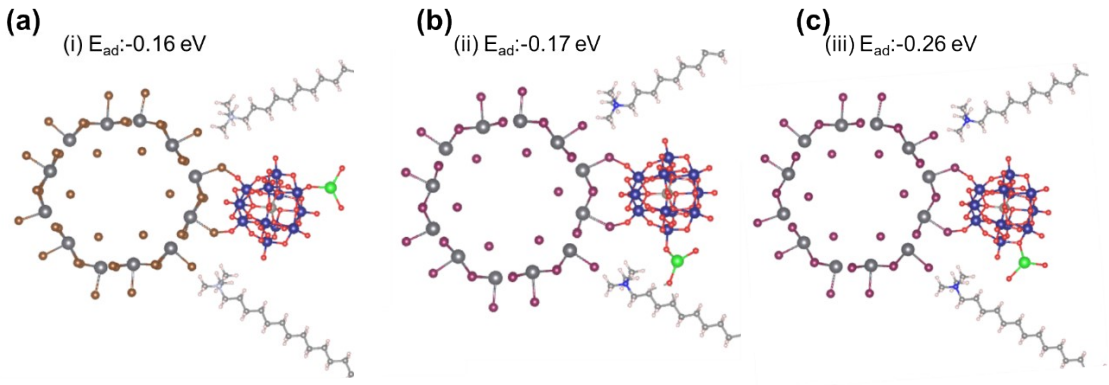

Fig. S14 Adsorption models for UO_2^{2+} on $(HMTA)_3Pb_2Br_7$@STA-PW_{12}.

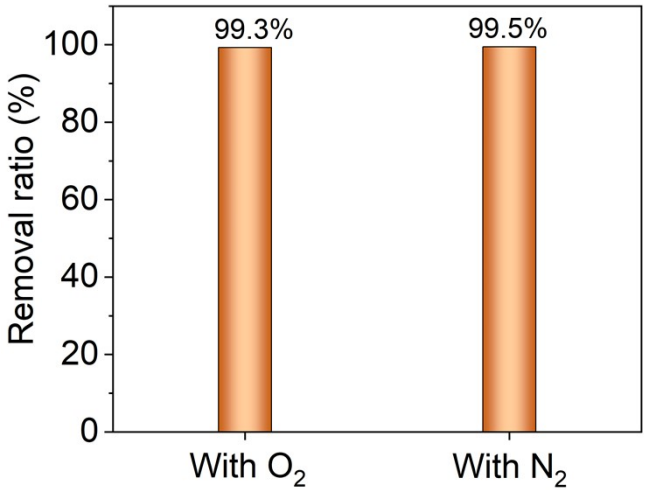

Fig. S15 Removal ratio of U(VI) under O_2 and N_2 atmosphere.

Table S1. Comparison of the durability of $(HMTA)_3Pb_2Br_7$@STA-PW_{12} in water with some selected perovskites.

Materials	Methods	Medium	Characterizations	Observed durability	Ref.
$MAPbBr_3$/SSDC (1.13 wt%)	Physical blending	Water	PL	36 h	1
$MAPbBr_3$-polystyrene	Swelling-deswelling microencapsulation	Boiling water	PL	30 min	2

Polyimide-coated $CsPbBr_3$ NCs	In situ growth	Water	PL	60 min	3
$CsPbBr_3/SiO_2$	Water-triggered transformation	Hexane/ water	PL	7 days	4
$CsPbBr_3@SiO_2$ NPs	Modified supersaturated recrystallization	Water	PL	40 min	5
Mesoporous SiO_2-$CsPbBr_3$@AlOx	Modified template assisted formation	Water	PL	8 h	6
$MAPbBr_3@SiO_2$/ PVDF films	Impregnation and physical blending	Water	PL	2 h	7
$CsPbBr_3$@ZnO nanoparticles	Physical blending	Water	PL	30 min	8
$Cs_2Sn_{0.89}Te_{0.11}Cl_6$	Hydrothermal method	Water	PXRD	360 min	9
$(HMTA)_3Pb_2Br_7$ @STA-PW_{12}	Conventional solution method	Water	PXRD	10 h	This work

References

[1] H. Wang, H. Lin, X. Piao, P. Tian, M. Fang, X. An, C. Luo, R. Qi, Y. Chen and H. Peng, Organometal halide perovskite nanocrystals embedded in silicone resins with bright luminescence and ultrastability, J. Mater. Chem. C, 2017, 5, 12044–12049.

[2] Y. Wang, J. He, H. Chen, J. Chen, R. Zhu, P. Ma, A. Towers, Y. Lin, A. J. Gesquiere, S. Wu and Y. Dong, Ultrastable, Highly Luminescent Organic–Inorganic Perovskite–Polymer Composite Films, Adv. Mater., 2016, 28, 10710–10717.

[3] J. Zhang, P. Jiang, Y. Wang, X. Liu, J. Ma and G. Tu, In Situ Synthesis of Ultrastable CsPbBr3 Perovskite Nanocrystals Coated with Polyimide in a CSTR System, ACS Appl. Mater. Interfaces, 2020, 12, 3080-3085.

[4] H. Hu, L. Wu, Y. Tan, Q. Zhong, M. Chen, Y. Qiu, D. Yang, B. Sun, Q. Zhang and Y. Yin, Interfacial Synthesis of Highly Stable CsPbX3/Oxide Janus Nanoparticles, J. Am. Chem. Soc., 2018, 140, 406–412.

[5] Q. Zhong, M. Cao, H. Hu, D. Yang, M. Chen, P. Li, L. Wu and Q. Zhang, One-Pot Synthesis of Highly Stable $CsPbBr_3$@SiO_2 Core-Shell Nanoparticles, ACS Nano, 2018, 12, 8579-8587.

[6] C.-Y. You, F.-M. Li, L.-H. Lin, J.-S. Lin, Q.-Q. Chen, P. M. Radjenovic, Z.-Q. Tian and J.-F. Li, Ultrastable monodispersed lead halide perovskite nanocrystals derived from interfacial compatibility, Nano Energy, 2020, 71, 104554.

[7] Y. Huang, F. Li, L. Qiu, F. Lin, Z. Lai, S. Wang, L. Lin, Y. Zhu, Y. Wang, Y. Jiang and X. Chen, Enhancing the Stability of $CH_3NH_3PbBr_3$ Nanoparticles Using Double Hydrophobic Shells of SiO_2 and Poly(vinylidene fluoride), ACS Appl. Mater. Interfaces, 2019, 11, 26384–26391.

[8] P. Song, B. Qiao, D. Song, J. Cao, Z. Shen, G. Zhang, Z. Xu, S. Zhao, S. Wageh and A. Al-Ghamdi, Enhancing the stability and water resistance of $CsPbBr_3$ perovskite nanocrystals by using tetrafluoride and zinc oxide as protective capsules, J. Mater. Sci., 2020, 55, 9739–9747.

[9] Z. Tan, Y. Chu, J. Chen, J. Li, G. Ji, G. Niu, L. Gao, Z. Xiao and J. Tang, Lead-Free Perovskite Variant Solid Solutions $Cs_2Sn_{1-x}Te_xCl_6$: Bright Luminescence and High Anti-Water Stability, Adv. Mater., 2020, 32, 2002443.